CHEMISTRY OF MATERIALS

Article

pubs.acs.org/cm

Atomic-Scale Tracking of a Phase Transition from Spinel to Rocksalt in Lithium Manganese Oxide

Peng Gao,*[,†,‡,§] Ryo Ishikawa,[†] Eita Tochigi,[†] Akihito Kumamoto,[†] Naoya Shibata,[†] and Yuichi Ikuhara*[,†,⊥,¶]

[†]Institute of Engineering Innovation, School of Engineering, The University of Tokyo, Tokyo 113-8656, Japan

[‡]Electron Microscopy Laboratory, School of Physics, and Center for Nanochemistry, Peking University, Beijing 100871, China

[§]Collaborative Innovation Center of Quantum Matter, Beijing 100871, China

[⊥]Nanostructures Research Laboratory, Japan Fine Ceramics Center, Atsuta, Nagoya 456-8587, Japan

[¶]World Premier International Research Center Initiative for Advanced Institute for Materials Research, Tohoku University, Sendai 980-8577, Japan

Supporting Information

ABSTRACT: For the intercalation type cathode in lithium-ion batteries, the structural framework of electrode is expected to remain unchanged during lithium insertion and extraction. Unfavorable phase transition in electrode materials, which has been frequently observed, modifies the structural framework, which leads to capacity loss and voltage decay. Here, we track atoms motion/shift in lithium manganese oxide during a phase transition from spinel to rocksalt by using atomically resolved aberration corrected scanning transmission electron microscopy and spectroscopy. We find that when given energy, the transition metal cation can readily hop between oxygen tetrahedral and octahedral sites in oxygen deficient lithium manganese oxide similar to lithium diffusion behavior, which leaves the anion structure framework almost unchanged. During this phase transition, the intermediate state, migration length, and atomic structure of phase boundaries are revealed, and the mechanism is discussed. Our observations help us to understand the past experimental phenomena and provide useful information to stabilize the structure of electrode materials and thus improve the cycling life of lithium-ion batteries.

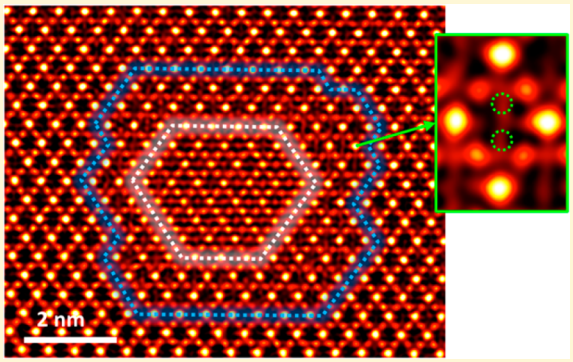

INTRODUCTION

In rechargeable lithium-ion batteries (LIBs), the host cathode material containing transition metal (TM) is expected to retain its structure framework during lithium insertion and extraction. However, many studies suggested that during electrochemical cycling the TM ions could also become active and move around[1−19] to form new structures or phases. Such unfavorable structure change or phase transition likely slows down the lithium diffusion or even blocks the diffusion channels, which subsequently have attributed to the capacity fading or voltage decay.[7,8,12] Especially in the manganese-containing cathode materials, the phase transition between layered, spinel, and rocksalt structures, which only involves TM and Li rearrangements but leaves anions sublattice structure framework almost unchanged, has been frequently observed on the surface or in the bulk upon electrochemical reactions.[3,5−19] By using X-ray absorption spectroscopy (XAS), Park et al. found that in layered $LiMnO_2$ the Mn ions can migrate to interlayer positions during lithium insertion and extraction and proposed that such a structure change accounts for the capacity loss.[7] Wagemaker et al. studied the $LiMg_{0.1}Ni_{0.4}Mn_{1.5}O_4$ spinel structure by using X-ray diffraction (XRD) and neutron diffraction (ND) and suggested that both Ni and Mn can migrate up to ∼10 nm in distance, which strongly influences on the cycling behavior.[8] More recently, similar structure change has been observed in various cathode materials, and similar mechanism involving Mn migration has been suggested by many groups based on the aberration corrected scanning transmission electron microscopy (STEM) observations of electrode materials (in particular on the surfaces) cycled at different charge/discharges states.[9−11,13−19] The high mobility of Mn ions originating from the low activation energy, for example, 0.2 eV for Mn migration in Li_xMnO_2, was reported by Reed et al. based on ab initio calculations.[20] Such a barrier height is even lower than typical barriers for Li diffusion in many cathode materials including $LiMn_2O_4$ (refs 21 and 22). Despite extensive studies on the configuration of reconstructed structures in cathode materials at electrochemical equilibrium states, during the phase transition, the TM cation migration path, intermediate state, migration length, and atomic and electronic structures of phase

Received: August 31, 2016
Revised: January 12, 2017
Published: January 13, 2017

DOI: 10.1021/acs.chemmater.6b03659
Chem. Mater. 2017, 29, 1006−1013

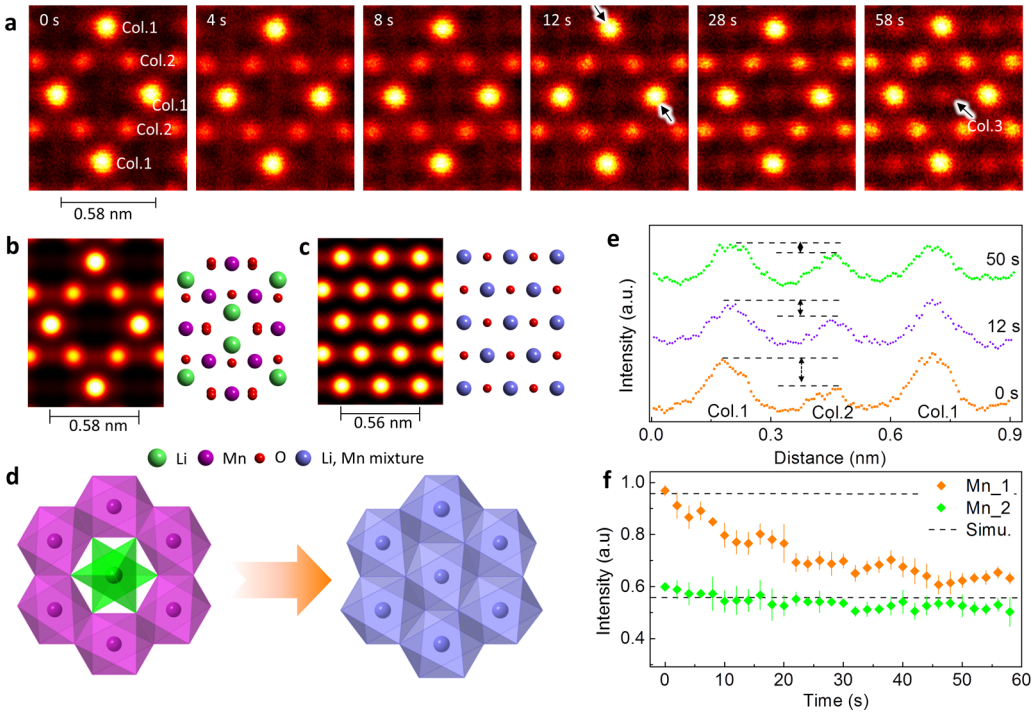

Figure 1. Evolution of atomic arrangements during phase transition from spinel to rocksalt in $LiMn_2O_{4-\delta}$ (LMO, δ denotes oxygen deficient). (a) Selected continuous HAADF-STEM images showing the phase transition from spinel to rocksalt in LMO. The viewing direction is $[110]_{spinel}$. The unoccupied column 3 in spinel becomes occupied in the rocksalt. These selected frames are unit-cell averaged from a region of 5 × 5 unit cells to reduce the noise. (b) Simulated HAADF-STEM image of spinel $LiMn_2O_4$ with thickness of 30 nm. The schematic is shown in the right. (c) Simulated HAADF-STEM image of rocksalt $LiMnO_2$ with thickness of 30 nm. The schematic is shown in the right. (d) Schematic showing tetrahedrally coordinated Li in the spinel phase becomes octahedral sited in the rocksalt phase after phase transition. (e) Selected intensity-profiles along the columns 1−2−1 direction indicated by black arrows in panel a. Orange: at 0 s (the 1st frame). Purple: at 12 s (the 7th frame). Green: at 50 s (the 26th frame). (f) Evolution of intensities of column 1 and 2 are plotted as a function of time. The values are averaged from four column 1 and four column 2 in a single unit cell shown in Figure S2. The dashed lines correspond to the simulation values of $LiMn_2O_4$ with thickness of 30 nm.

boundaries, however, are still largely unknown. Revealing these details during structural changes is vital to understand why the electrodes fail and thereby how we can improve them.

Here we study the dynamic process of the phase transition from spinel to rocksalt in lithium manganese oxide $LiMn_2O_{4-\delta}$ (LMO, $\delta \approx 0.1$, δ denotes oxygen deficient and oxygen vacancy concentration was determined by heat capacity measurement described in the Experimental Section). We choose the oxygen deficient cathode material because previous calculations suggested that the oxygen vacancy can reduce the barrier for Mn diffusion and thereby facilitate the phase transition.[14] This theory seems in good agreement with experimental results that structure reconstructions commonly occur at the surfaces of oxide electrode materials (refs 3, 9−11, 13, 15, 17, 19, and literature therein) where formation energy of oxygen vacancies is typically lower. Therefore, the chosen oxygen deficient LMO can closely represent the structurally active surface of cathode materials in practical batteries and give us more precise knowledge on the relation between structure and properties. To monitor the atom motions during phase transition, electron probe in aberration corrected STEM operated at 200 kV or 300 kV was focused on a small thin region of LMO particle to provide energy to overcome the diffusion barrier via electron−atom elastic collision mechanism to drive the phase transition (see Supporting Discussion for details). This technique, atoms gaining energy from electron probe to overcome barriers for diffusion, has already been widely used to study dynamics of single dopant and defects motion[23,24] and phase transition in a variety of material systems.[25−29]

We find that the phase transition from spinel to rocksalt in LMO involves tetrahedral coordinated Li migrates to the neighboring face-shared empty octahedron, $Li_{tet} \rightarrow Li_{oct}$ (the subscript "tet" denotes an occupation site of oxygen tetrahedron, and "oct" denotes an occupation site of oxygen octahedron hereinafter), whereas octahedrally sited Mn migrates to the neighboring edged-shared empty octahedron and passes through a tetrahedral site as an intermediate state, $Mn_{oct} \rightarrow Mn_{tet} \rightarrow Mn_{oct}$. Meanwhile, the O slightly shifts to high symmetric positions, $O_{\text{low symmetric position}} \rightarrow O_{\text{high symmetric position}}$, but the entire anion structure framework remains basically unchanged. During phase transition, the changes in chemical environments for Li and Mn are further confirmed by the electron energy loss spectroscopy (EELS). In addition, the phase boundary between the newly create rocksalt and parent spinel matrix is ∼1−3 unit cells wide. Various cationic configurations coexist in the phase boundary including Li_{tet}, $Li_{vacancy}$, Li_{oct}, Mn_{tet}, $Mn_{vacancy}$, and Mn_{oct}. Although the spinel phase is usually considered as a stable structure, our observations indicate that the TM atoms in the oxygen deficient spinel cathode host can have similar diffusion behavior with alkali-metal Li, leading to unfavorable structure modification that likely degrades the performance of battery as the lithium channels can be blocked by the unexpected TM cation occupations. These results can help us to understand the past experimental phenomena and also provide useful insights into engineering of LIB electrode materials such as elemental doping or surface modification to stabilize the TM structure framework.

DOI: 10.1021/acs.chemmater.6b03659
Chem. Mater. 2017, 29, 1006−1013

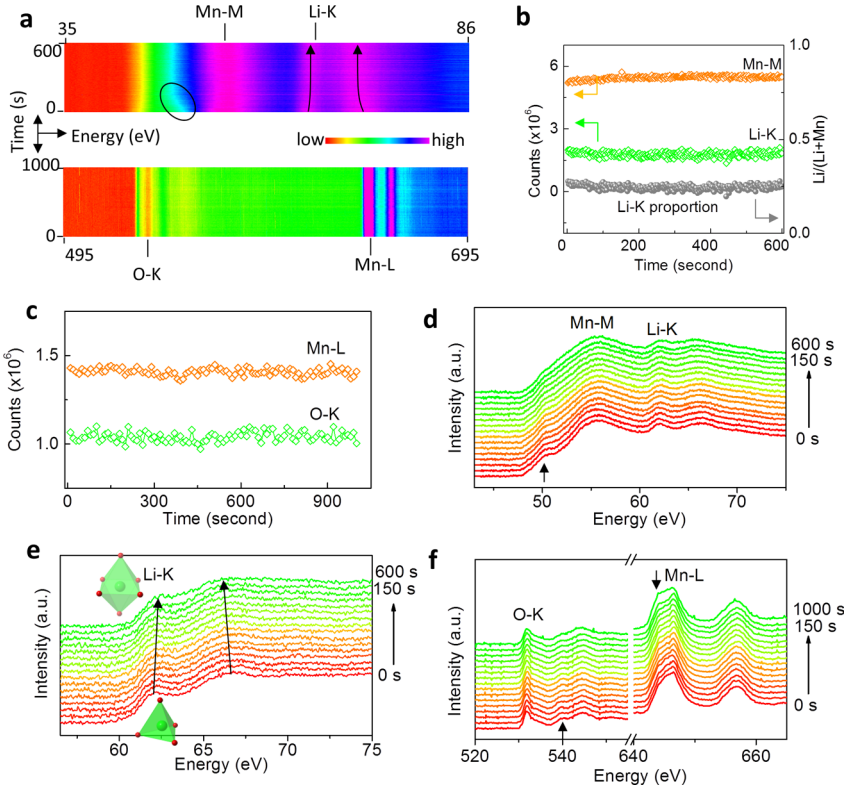

Figure 2. Time-sequence electron energy loss spectra (EELS) showing the chemical evolution during phase transition from spinel to rocksalt in LMO. (a) 2D EELS maps showing the chemical evolution of Mn−M, Li−K, O−K, and Mn−L edges. The black circle highlighting a change in the Mn−M edge during phase transition. The black arrows indicate the peaks shift in Li−K edge during phase transition. (b) Integrated intensities of simultaneously recorded Li−K and Mn−M edges. Li proportion is also plotted as a function of time. No obvious mass loss in Li or Mn is observed even after 600 s. (c) Integrated intensities of simultaneously recorded O−K and Mn−M are plotted as a function of time. No obvious mass change in O or Mn is observed even after 1000 s, indicating only atomic rearrangements take place during phase transition. (d) Evolution of Mn−M edge during phase transition. The pre-edge peak in Mn−M indicated by the arrow becomes less pronounced upon phase change. No obvious change is observed after 150 s. (e) Evolution of Li−K edge. The left peak slightly shifts to right, and right peak slightly shifts to left during $Li_{tet} \rightarrow Li_{oct}$. (f) Evolution of O−K edge and Mn−L edges. Upon phase transition, the small peak of O−K edge at ∼540 eV becomes less pronounced, and the left shoulder of Mn−L_3 edge becomes intense. No significant peak shift is observed.

RESULTS AND DISCUSSION

Evolution of Atomic Arrangements during Phase Transition. Selected continuous high angle annular dark-field (HAADF)-STEM images in Figure 1a show the phase transition from spinel to rock salt in $LiMn_2O_{4-\delta}$ along the viewing direction of $[110]_{spinel}$ (the structure information is listed in the Table S1). The atomic arrangements of spinel and rocksalt phases in experimental images are in good agreement with the simulated images in Figure 1b and c, respectively. In the spinel structure, the Li is tetrahedrally coordinated (Li_{tet}), whereas in the rocksalt, both Li and Mn are octahedral sited (Li_{oct} and Mn_{oct}), as schematically displayed in Figure 1d. In this viewing direction, the Mn density of column 1 in spinel structure is twice of column 2, whereas in the rocksalt phase, the density of all cation columns is the same. Upon phase transition, the contrast of column 3 gradually becomes intense (see Figure S1), the absolute intensity of column 1 is significantly reduced, but the reduction of column 2 in intensity is subtle in Figure 1e and f, suggesting partial Mn cations moves from column 1 to column 3 (see also Figure S2) and Mn density in column 2 remains almost unchanged. Besides, the Li at the Li column (or referred as column 4 hereinafter), that is, Li_{tet}, is supposed to uniformly distribute to columns 1, 2 and 3, forming mixture of cations as all the cation columns in rocksalt structure are equal in this viewing direction. However, since the contrast in the (Li, Mn) mixture columns are dominated by the relatively heavier Mn in the STEM images, Li motion cannot be directly captured. On the other hand, because of the strong Coulomb interaction between Li and Mn, the configuration of Li_{tet} with two Mn_{oct} neighbors is very unstable,[1] further confirming Mn rearrangement drives Li migration. Meanwhile, the O columns also slightly shift away from the Mn column 1 to higher symmetric positions upon phase transition, which is clearly confirmed by simultaneously recorded annular bright-field (ABF) images and simulations in Figure S3.

Evolution of Electronic Structures during Phase Transition. Time-sequence electron energy loss spectra (EELS, see also Figure S4) are also recorded to monitor the evolutions of composition and chemical environments (in Figure 2a) upon phase transition. The integrated intensity of Li−K (in Figure S5) and Mn−M edges from the same spectra in Figure 2b does not show any significant mass loss of Mn or Li. The same conclusion is obtained from the integrated intensity of Mn−L and O−K edges in Figure 2c. On the other hand, for respective cations the change in chemical environments upon phase transition leads to the changes in the energy loss near-edge fine structures. The prepeak of Mn−M edge indicated by the arrow in Figure 2d becomes decreased after 150 s, corresponding to the change highlighted by the dark circle in the 2D-EELS map in Figure 2a (see also Figure S6).

DOI: 10.1021/acs.chemmater.6b03659
Chem. Mater. 2017, 29, 1006−1013

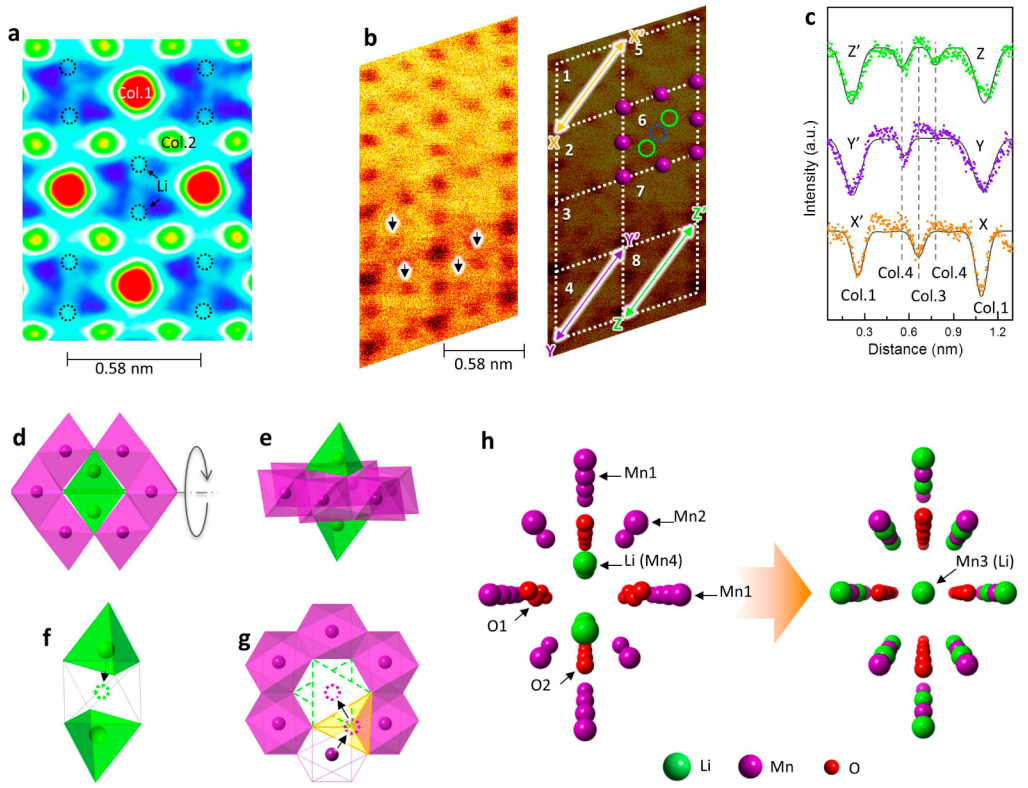

Figure 3. Intermediate structure and atom motion pathways during phase transition from spinel to rocksalt. (a) Brightness, contrast, and smoothness adjusted HAADF image at 8 s (5th frame) in Figure 1a. At this stage, the increased intensity in Li columns (indicated by dashed circles) is due to the occupation of heavier Mn. (b) A fast scanned ABF image showing occupation of Mn atoms at the Li columns indicated by the black thin arrows. Labels are listed in the right insert. (c) Intensity line profiles along the XX′, YY′, and ZZ′ indicated in panel b. In the first diamond along XX′, the column 3 is partially occupied, indicating a rocksalt configuration. In the fourth diamond along YY′, the left Li column is heavily occupied by Mn, whereas the right one is almost unoccupied, indicating intermediate states with local ordering of Mn occupation and heterogeneity. In the eighth diamond ZZ′, the two Li columns are almost evenly occupied by Mn. (d) A spinel cluster along $[110]_{spinel}$ direction. (e) Side view of the same cluster. (f) Li jumps from the tetrahedral site to the neighboring empty octahedral site during phase transition. (g) Mn diffusion between octahedral sites passes though a tetrahedral site as intermediate state. The viewing direction is $[111]_{spinel}$. (h) A perspective view of spinel $LiMn_2O_4$ along [110] direction and rock salt $LiMnO_2$. In the spinel phase, the atom density of column 1 is twice of column 2. In the rock salt phase, the atom densities of columns 1, 2, and 3 are the same. Original Li sites are no longer occupied in the rocksalt phase.

Generally, such disappearance of the prepeak is attributed to the reduction of TM elements. Since no distinguishable loss of anions is observed during the phase transition in Figure 2c, the change in Mn−M edge should result from the rearrangements of Li and Mn, for example, part of Mn atoms intermediately stay at tetrahedral sites (we will discuss it again below). In addition, Li migration from tetrahedral to octahedral sites may also indirectly alter the interactions between Mn and O. In the rocksalt phase the Li_{oct} interacts with more negative charge than Li_{tet} in the spinel structure and therefore less negative charge interacts with the Mn after phase transition. After 150 s, no significant changes in the edges are observed, suggesting no further atomic rearrangements happens and the newly formed rocksalt phase is stable. From the Li−K edge in Figure 2e, the groove between two peaks becomes narrower and less invisible as the left peak shifts to right and the right peak shifts to left. Such peak shift is also visible in the 2D-EELS map in Figure 2a, which is highlighted by the arrows. Since all the spectra are precisely calibrated with the simultaneously recorded zero loss peaks, these subtle peak shifts in the Li−K edge should come from the Li chemical environmental changes instead of errors. Such a change is a characteristic of $Li_{tet} \rightarrow Li_{oct}$, which was suggested by previous experimental and simulated Li−K edges in Li−Ti−O system.[27] In O−K and Mn−L edges recorded from another region, within the first 150 s, the small peak of O−K (indicated by the arrow in Figure 2f) becomes less pronounced, while left shoulder of Mn−L_3 becomes more intense. The later feature is also in good agreement in previous X-ray absorption spectroscopy (XAS) study[3] that suggested the increased left shoulder of Mn−L_3 is due to the formation of rocksalt surface layer in $LiNi_xMn_xCo_{1-2x}O_2$ during electrochemical cycling.

Intermediate Structures. During phase transition, the intensity at Li columns (or column 4) in the HAADF image becomes intense first and then fades away in Figure 1a. Figure 3a is the brightness/contrast and smooth adjusted HAADF image at 8 s, in which the dashed black circles highlight that the Li columns are partially occupied by heavier Mn ions (Mn_{tet}), otherwise no bright contrast is expected from the Li columns as Li is too light to be visible in Z-contrast image. At the end of phase transition, the Z-contrast at the Li columns disappears completely, indicating these partial Mn-occupation at Li columns (Mn_{tet}) are only intermediate states during phase transition. Previous ab initio calculation suggests the barrier for Mn diffusion to adjacent tetrahedral sites could be quit low, that is, ∼0.2 eV in the case of Li_xMnO_2 in ref 20. As a result, at the initial stage of phase transition within the first 8 s, partial Mn atoms readily migrate into tetrahedral sites ($Mn_{oct} \rightarrow$

DOI: 10.1021/acs.chemmater.6b03659
Chem. Mater. 2017, 29, 1006−1013

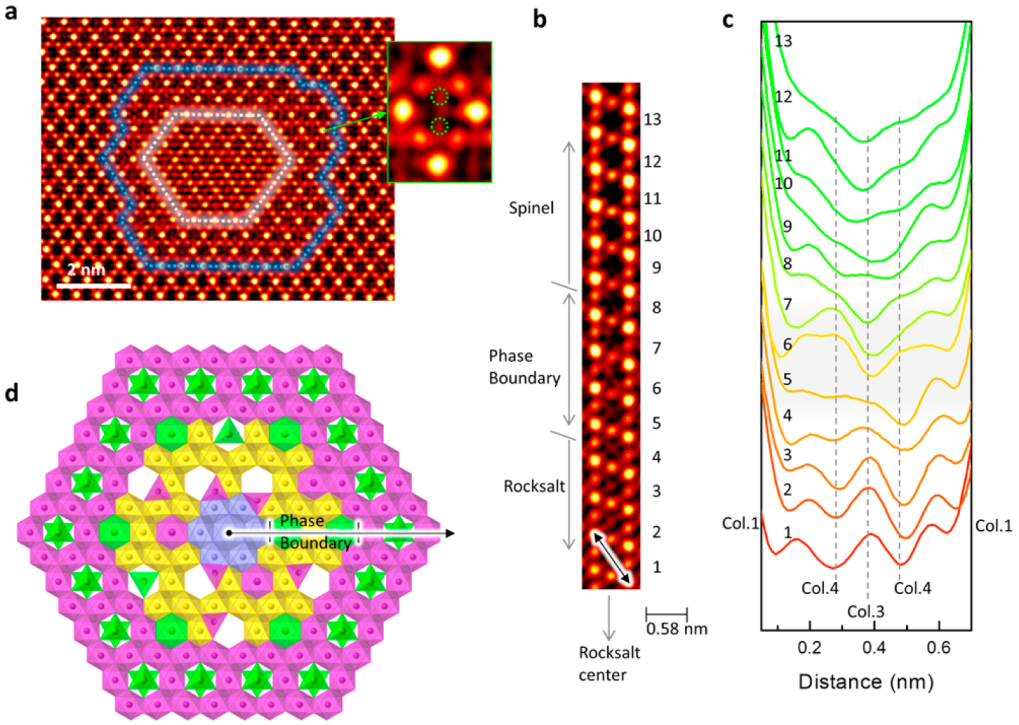

Figure 4. Atomic structure of phase boundary between newly formed rocksalt and parent spinel matrix. (a) Lower magnification of a HAADF-STEM image containing a precreated rocksalt phase domain highlighted by the dashed white line. This image is filtered in Fourier space by removing low and high frequency noises as shown in Figure S7. A transition zone between the dashed white and blue lines is considered as the phase boundary. The right inset showing the phase boundary contains intermediate structure Mn_{tet}. (b) A selected atom row and (c) corresponding intensity line profiles along long diagonal direction of diamond across the phase boundary. The intensity of column 3 becomes weaker far way from the rocksalt phase center. At the phase boundary, that is, in the fifth, sixth, and seventh diamonds, the Li columns are partially and unevenly occupied by Mn, indicating an intermediate states zone with local ordering and heterogeneity of Mn_{tet}. (d) Atomistic illustration of phase boundary between spinel and rocksalt phases. The viewing direction is $[111]_{spinel}$. Various structure configurations exist in the boundary including Li_{tet}, $Li_{vacancy}$, Li_{oct}, Mn_{tet}, $Mn_{vacancy}$, and Mn_{oct}. Cation vacancies and anions are not shown for clarity.

Mn_{tet}), forming a Mn_3O_4-like structure. Such Mn_3O_4-like structure, Mn_{tet}, also has been observed at the interface of the $LiMn_2O_4$ thin films on Au substrate in our previous study.[30] A single fast scanned ABF image in Figure 3b contains both Mn_{tet} and Mn_{oct} configurations. The intensity line profiles plotted in Figure 3c unambiguously show there is some local ordering of intermediate Mn_{tet}. The structure in No. 1 unit cell is rocksalt-like as the profile along XX′ shows only the middle column is partially occupied. Along YY′ in No. 4 unit cell, the left Li column is highly occupied by Mn whereas the right column is barely occupied, and along ZZ′ in unit cell No. 8, the left and right Li columns are almost evenly occupied by Mn, indicating local ordering and heterogeneity in distribution. In addition, both our previous observation[30] and this study confirm that this intermediate Mn_{tet} in Mn_3O_4-like structure can be stable, although theoretical predication suggested that Mn_{tet} is metastable in Li−Ni−Mn-O cathode.[14]

On the basis of these observations, the atom migration paths during phase transition can be extracted for both of Li and Mn. Figure 3d shows a small cluster of spinel LMO seen along $[110]_{spinel}$. These six Mn octahedron forms a loop, leaving an empty octahedron in the center in Figure 3e. This empty octahedron is also sandwiched by two Li tetrahedrons and shares planes with the Li tetrahedrons and edges with the six Mn octahedrons. Upon phase transition, Li jumps to the empty octahedral site and leaves a Li vacancy at the tetrahedral site. Indeed, during electrochemical reactions in $LiMn_2O_4$ electrode, the Li diffusion from one tetrahedral site to anther also has to pass through this empty octahedral site. The barrier for $Li_{tet} \rightarrow Li_{oct}$ is ∼0.5 eV (refs 21 and 22). For Mn motion path, since in both spinel and rocksalt phases the Mn atoms are octahedrally coordinated, one of these six Mn atoms jumps to the central empty octahedron upon phase transition. Instead of a direct jump, the Mn will first migrate to the neighboring tetrahedral site ($Mn_{oct} \rightarrow Mn_{tet}$) as an intermediate state shown in Figure 3a and b. This intermediate Mn_{tet} shares faces with both the original and empty octahedrons, as shown in Figure 3g. Along the $[110]_{spinel}$ direction, the intermediate tetrahedral site (Mn_{tet}) shares the same column with tetrahedrally coordinated Li. As a result, the Li columns appear partially occupied by heavier Mn at the initial stage of phase transition. This move, $Mn_{oct} \rightarrow Mn_{tet}$, is fast as in Figure 1a; after 8 s, the contrast in the Li columns (column 4) becomes weaker, indicating the start of the second stage that Mn atoms move to neighboring empty octahedral sites to form new rocksalt structure ($Mn_{tet} \rightarrow Mn_{oct}$). The fast $Mn_{oct} \rightarrow Mn_{tet}$ and relatively slow $Mn_{tet} \rightarrow Mn_{oct}$ have been predicted in Li_xMnO_2 by ab initio calculation.[20] The atom motion is summarized in Figure 3h with three-dimensional perspective view.

Phase Boundary. Another issue is the atomic structure of phase boundary between spinel and rocksalt. Figure 4 is a filtered HAADF-STEM image (see also Figure S7) containing a precreated rocksalt phase domain that is highlighted by the dashed white line. The matrix is the parent spinel phase, while the core is rocksalt phase. A transition zone between these two phases is considered as the phase boundary, which is rich in the

DOI: 10.1021/acs.chemmater.6b03659
Chem. Mater. 2017, 29, 1006−1013

intermediate structure of Mn_{tet}, as shown in Figure 4b and c. The thickness of the boundary is ~1−3 unit cells. Therefore, an atomistic model of the phase boundary can be proposed in Figure 4d, where various structures exist in the phase boundary including Li_{tet}, $Li_{vacancy}$, Li_{oct}, Mn_{tet}, $Mn_{vacancy}$, and Mn_{oct}.

DISCUSSION

Both spinel and rocksalt structures of Li−Mn−O systems have the same ABC close-packed anions stacking sequence, and therefore, the oxygen framework can remain basically unchanged except subtle shift during a phase transition. In this regard, we can consider both Li and Mn cations are accommodated in the anion sublattice framework and the cations can occupy different sites to form different phases. For both Li and Mn atoms, their migration behavior is determined by their respective diffusion barriers respect to external excitations. Once the barrier for Mn migration is close to or smaller than that for lithium diffusion, the Mn diffusion takes place during electrochemical cycling, leading to formation of unexpected new phases. Among of these structures, in the case of oxygen deficient samples, the rocksalt phase with disordered cations arrangements seems to be the most stable one as rocksalt has been frequently observed in many cathode materials (refs 1, 3, 9, 10, 19, and literature therein).

On the other hand, during electrochemical cycling, the barrier for cation diffusion could be very different as the barrier significantly depends on lithium concentration[20] and neighboring cationic configurations,[31] which suggest that the diffusion behavior is very complicate in the real battery cells. Previous calculation reported the typical barrier for Li diffusion is ~0.5 eV in $LiMn_2O_4$ (refs 21 and 22). Another calculation example of Li_xMnO_2 (ref 20, the average valence is 3+ for Mn) suggested the barrier for $Mn_{oct} \rightarrow Mn_{tet}$ is ~0.2 eV, which is even less than half of the lithium diffusion barrier for $Li_{tet} \rightarrow Li_{oct}$, indicating Mn diffusion can be even more energetically favorable in some cases. In our study (the average valence is 3.4+ for Mn in the $LiMn_2O_{3.9}$, see also the details in the Experimental Section), besides the diffusion barrier, the cation migration also depends on the energy gained from atom-electron interaction. Assuming the diffusion barriers for both Li and Mn are 0.5 eV, the calculation based on pure elastic collision[23] shows that diffusion possibility for Mn is about 10-times that for Li, indicating Mn is more active and Mn rearrangement likely takes place prior to Li motion. More details are included in the Supporting Information, Figures S8−S10.

In addition, by introducing the O vacancies in $Li_{20/28}Ni_{1/4}Mn_{7/12}O_2$ (ref 14, the valence is 4+ for Mn), the barrier for $Mn_{oct} \rightarrow Mn_{tet}$ can be reduced from 2.6 to 0.7 eV (about four-times lower), meaning the oxygen vacancy would significantly destabilize TM structure framework and facilitate the phase transition. Note that in all of the TM oxides the surface is always O deficient due to asymmetric bonding between cations and O on surface, and thus, the oxygen can be readily released to form vacancies,[33] especially in the low oxygen pressure environments in the battery cells, which are usually fabricated in the argon-filled glovebox. This explains the structure reconstruction is frequently observed on the surface rather than the interior of bulk. Moreover, these results imply that we can stabilize the spinel phase in the battery electrode materials and prevent the phase transition by reducing the concentration of oxygen vacancies.

Beside Mn-containing cathode materials, other TM cations diffusion phenomena have also been reported including Ni (refs 8 and 14), Cr (ref 1), Mo (refs 1 and 2), and Fe (ref 4). This seems a more general issue for the TM-containing cathode materials. Previous studies from neutron powder diffraction[12] and electrochemical measurements[32] also discussed the lithium and TM ions migration paths and showed that such unexpected structural rearrangement can induced capacity loss and voltage-fade in batteries. Partial substitution with other TM ions by hindering the TM migration,[7] or increasing the TM diffusion barrier[14] via reducing concentration of oxygen vacancies, may help to stabilize the structures.

CONCLUSION

In summary, we use aberration corrected STEM imaging and spectroscopy to monitor a phase transition in a cathode LMO. The cations migration and anions shift, that is, $Li_{tet} \rightarrow Li_{oct}$, $Mn_{oct} \rightarrow Mn_{tet} \rightarrow Mn_{oct}$, and $O_{low\ symmetric\ site} \rightarrow O_{high\ symmetric\ site}$, induces a phase transition from spinel to rocksalt, while it leaves the oxygen sublattice framework almost unchanged. The phase boundary between the newly formed rocksalt and parent spinel matrix is not atomically sharp instead in a thickness ~1−3 unit cells. Various structure configurations exist in the phase boundary, for example, the intermediate structure of Mn_{tet}, which seems stable. Note that TM diffusion is a general issue for cathode materials, the atomic-scale monitoring of the TM diffusion dynamic process and evolution of chemical environments in our work impart useful knowledge for understanding the degradation mechanism for LIB electrode materials. Moreover, unlike the X-ray diffraction, absorption spectroscopy, or nuclear magnetic resonance, direct observation based on aberration corrected STEM imaging (both HAADF and ABF) and EELS demonstrated herein allows atoms motions tracked during solid state phase transformations, providing unprecedented opportunities to study a variety of functional materials for energy, and solid-state physics and chemistry.

EXPERIMENTAL SECTION

Commercial $LiMn_2O_4$ particles were synthesized by sintering Li_2CO_3 and $MnCO_3$ at high temperature (provided by Toshima Co., Japan). At the surface of oxides, the oxygen vacancies can naturally form due to weak bonding (with dangling bonds).[33] To facilitate the phase transition, the commercial particles were annealed in N_2 at 700 °C to create higher concentration of oxygen vacancies in our laboratory, forming $LiMn_2O_{4-\delta}$, where δ denotes the oxygen deficient. Note that the oxygen vacancies can readily form at such high temperature and low oxygen pressure. To determine the oxygen vacancy concentration, we performed heat capacity measurement and δ is estimated to be 0.1 by referring the previous report,[34] which corresponds to 2.5% oxygen deficiency (see Supporting Figure S11). According to the previous report,[14] 2−4% oxygen deficiency gives a significant reduction in the Mn diffusion barrier (from 2.6 to 0.7 eV). With the oxygen vacancies, the diffusion barrier for Li is also likely reduced. The stoichiometric compositions of spinel and rocksalt can be given as $LiMn_2O_4$ and $Li_2Mn_2O_4$, respectively. In our experiments, the oxygen deficient spinel $LiMn_2O_{4-\delta}$ can be rewritten as $Li_{2-x}Mn_2O_{4-\delta}$ with $x = 1$. After phase transition, the rocksalt can be written as $(Li, Mn)_{4-x}O_{4-\delta}$ with about 23% deficiency of cations sites. Note that we do not break the conservation of matter in above discussion. HAADF and ABF images are recorded simultaneously in probe-corrected cold-FEG JEMs at 200 kV (ARM200CF, JEOL Ltd.) and 300 kV (ARM300CF, JEOL Ltd.). The convergence semiangle for imaging is 24 mrad, collection semiangles spanning 65−240 mrad for ADF and 12−24 mrad for ABF imaging, respectively. We have sequentially acquired image, where the

DOI: 10.1021/acs.chemmater.6b03659
Chem. Mater. 2017, 29, 1006−1013

frame time-interval is typically ~2 s and the image size is 1024 by 1024 pixel.[23] A post drift correction based on the cross-correlation method was applied to align all the frames. To correct the energy drift, the EEL spectra were recorded by Dual EELS mode with Enfinium camera (Gatan Inc.) at 200 kV (ARM200CF, JEOL Ltd.), where the convergence semiangle is 24 mrad and collection angle 53 mrad. Multislice simulation of ABF images were carried out by using commercial software from HREM Research, Inc. The inner and outer angles were set to 12−24 mrad for the ABF detector, and the aperture was set to 24 mrad. The total Debye−Waller factors for both spinel and rocksalt are set as one. Different thicknesses were tested and compared with experimental images to find the most suitable thickness value of 30 nm.

■ ASSOCIATED CONTENT

Supporting Information

The Supporting Information is available free of charge on the ACS Publications website at DOI: 10.1021/acs.chemmater.6b03659.

Crystallography parameters of spinel and rocksalt phases of lithium manganese oxide; intensity-profiles of atom columns; contrast evolution in single unit cell during phase transition; oxygen shift during phase transition from spinel to rocksalt; time-sequence EEL spectra monitoring the phase transition; extraction of Li−K edge; EELS evolution under different defocus; mask for removal of high and low frequencies in the atomically resolved HAADF-STEM image; transfer energy for Li and Mn at different scattering angle; Mott cross-section of single Li and Mn atoms; total cross-section for Li and Mn; heat capacity of $LiMn_2O_{4-\delta}$; discussion of gaining energy, phase transition, and mass loss (PDF)

■ AUTHOR INFORMATION

Corresponding Authors

*E-mail: p-gao@pku.edu.cn.
*E-mail: ikuhara@sigma.t.u-tokyo.ac.jp.

ORCID

Peng Gao: 0000-0003-0860-5525

Notes

The authors declare no competing financial interest.

■ ACKNOWLEDGMENTS

P.G. acknowledges Joshua Hoemke for the sample annealing and heat capacity measurements. This work was supported in part by the Grants-in-Aid for Scientific Research on Innovative Areas "Nano Informatics" (Grant No. 25106003) from Japan Society for the Promotion of Science (JSPS), Grants-in-Aid for Scientific Research (A) (15H02290) from JSPS, and "Nanotechnology Platform" (Project No. 12024046) from the Ministry of Education, Culture, Sports, Science, and Technology in Japan (MEXT). P.G. was supported as a JSPS fellow for part of this work. P.G. also acknowledges the support from the National Natural Science Foundation of China (51502007, 51672007) and "2011 Program" Peking-Tsinghua-IOP Collaborative Innovation Center of Quantum Matter.

■ REFERENCES

(1) Lee, J.; Urban, A.; Li, X.; Su, D.; Hautier, G.; Ceder, G. Unlocking the Potential of Cation-Disordered Oxides for Rechargeable Lithium Batteries. *Science* **2014**, *343*, 519−522.

(2) Zhou, Y.-N.; Ma, J.; Hu, E.; Yu, X.; Gu, L.; Nam, K.-W.; Chen, L.; Wang, Z.; Yang, X.-Q. Tuning charge-discharge induced unit cell breathing in layer-structured cathode materials for lithium-ion batteries. *Nat. Commun.* **2014**, *5*, 5381.

(3) Lin, F.; Markus, I. M.; Nordlund, D.; Weng, T.-C.; Asta, M. D.; Xin, H. L.; Doeff, M. M. Surface reconstruction and chemical evolution of stoichiometric layered cathode materials for lithium-ion batteries. *Nat. Commun.* **2014**, *5*, 3529.

(4) Thackeray, M. M. Spinel electrodes for lithium batteries. *J. Am. Ceram. Soc.* **1999**, *82*, 3347−3354.

(5) Hwang, S. J.; Park, H. S.; Choy, J. H.; Campet, G. Evolution of local structure around manganese in layered $LiMnO_2$ upon chemical and electrochemical delithiation/relithiation. *Chem. Mater.* **2000**, *12*, 1818−1826.

(6) Hwang, S. J.; Park, H. S.; Choy, J. H.; Campet, G. Variation of the chemical bonding nature of $LiMn_{2-x}Ni_xO_4$ spinel oxides upon delithiation and lithiation reactions. *J. Phys. Chem. B* **2001**, *105*, 335−342.

(7) Park, H. S.; Hwang, S. J.; Choy, J. H. Relationship between chemical bonding character and electrochemical performance in nickel-substituted lithium manganese oxides. *J. Phys. Chem. B* **2001**, *105*, 4860−4866.

(8) Wagemaker, M.; Ooms, F. G. B.; Kelder, E. M.; Schoonman, J.; Mulder, F. M. Extensive migration of Ni and Mn by lithiation of ordered $LiMg_{0.1}Ni_{0.4}Mn_{1.5}O_4$ spinel. *J. Am. Chem. Soc.* **2004**, *126*, 13526−13533.

(9) Xu, B.; Fell, C. R.; Chi, M.; Meng, Y. S. Identifying surface structural changes in layered Li-excess nickel manganese oxides in high voltage lithium ion batteries: A joint experimental and theoretical study. *Energy Environ. Sci.* **2011**, *4*, 2223−2233.

(10) Boulineau, A.; Simonin, L.; Colin, J. F.; Bourbon, C.; Patoux, S. First Evidence of Manganese-Nickel Segregation and Densification upon Cycling in Li-Rich Layered Oxides for Lithium Batteries. *Nano Lett.* **2013**, *13*, 3857−3863.

(11) Huang, R.; Ikuhara, Y. H.; Mizoguchi, T.; Findlay, S. D.; Kuwabara, A.; Fisher, C. A. J.; Moriwake, H.; Oki, H.; Hirayama, T.; Ikuhara, Y. Oxygen-vacancy ordering at surfaces of lithium manganese (III, IV) oxide spinel nanoparticles. *Angew. Chem., Int. Ed.* **2011**, *50*, 3053−3057.

(12) Mohanty, D.; Li, J. L.; Abraham, D. P.; Huq, A.; Payzant, E. A.; Wood, D. L.; Daniel, C. Unraveling the Voltage-Fade Mechanism in High-Energy-Density Lithium-Ion Batteries: Origin of the Tetrahedral Cations for Spinel Conversion. *Chem. Mater.* **2014**, *26*, 6272−6280.

(13) Tang, D.; Sun, Y.; Yang, Z.; Ben, L.; Gu, L.; Huang, X. Surface Structure Evolution of $LiMn_2O_4$ Cathode Material upon Charge/Discharge. *Chem. Mater.* **2014**, *26*, 3535−3543.

(14) Qian, D. N.; Xu, B.; Chi, M. F.; Meng, Y. S. Uncovering the roles of oxygen vacancies in cation migration in lithium excess layered oxides. *Phys. Chem. Chem. Phys.* **2014**, *16*, 14665−14668.

(15) Tang, D.; Ben, L.; Sun, Y.; Chen, B.; Yang, Z.; Gu, L.; Huang, X. Electrochemical behavior and surface structural change of $LiMn_2O_4$ charged to 5.1 V. *J. Mater. Chem. A* **2014**, *2*, 14519−14527.

(16) Wu, Y.; Ma, C.; Yang, J. H.; Li, Z. C.; Allard, L. F.; Liang, C. D.; Chi, M. F. Probing the initiation of voltage decay in Li-rich layered cathode materials at the atomic scale. *J. Mater. Chem. A* **2015**, *3*, 5385−5391.

(17) Lin, M.; Ben, L.; Sun, Y.; Wang, H.; Yang, Z.; Gu, L.; Yu, X.; Yang, X.-Q.; Zhao, H.; Yu, R.; Armand, M.; Huang, X. Insight into the Atomic Structure of High-Voltage Spinel $LiNiO_3Mn_{1.5}O_4$ Cathode Material in the First Cycle. *Chem. Mater.* **2015**, *27*, 292−303.

(18) Zheng, S.; Huang, R.; Makimura, Y.; Ukyo, Y.; Fisher, C. A. J.; Hirayama, T.; Ikuhara, Y. Microstructural changes in $Li-Ni_{0.8}Co_{0.15}Al_{0.05}O_2$ positive electrode material during the first cycle. *J. Electrochem. Soc.* **2011**, *158*, A357−A362.

(19) Yan, P. F.; Nie, A. M.; Zheng, J. M.; Zhou, Y. G.; Lu, D. P.; Zhang, X. F.; Xu, R.; Belharouak, I.; Zu, X. T.; Xiao, J.; Amine, K.; Liu, J.; Gao, F.; Shahbazian-Yassar, R.; Zhang, J. G.; Wang, C. M. Evolution of Lattice Structure and Chemical Composition of the Surface Reconstruction Layer in $Li_{1.2}Ni_{0.2}Mn_{0.6}O_2$ Cathode Material for Lithium Ion Batteries. *Nano Lett.* **2015**, *15*, 514−522.

DOI: 10.1021/acs.chemmater.6b03659
Chem. Mater. 2017, 29, 1006−1013

(20) Reed, J.; Ceder, G.; Van der Ven, A. Layered-to-spinel phase transition in Li_xMnO_2. *Electrochem. Solid-State Lett.* **2001**, *4*, A78−A81.
(21) Verhoeven, V. W. J.; de Schepper, I. M.; Nachtegaal, G.; Kentgens, A. P. M.; Kelder, E. M.; Schoonman, J.; Mulder, F. M. Lithium dynamics in $LiMn_2O_4$ probed directly by two-dimensional ^7Li NMR. *Phys. Rev. Lett.* **2001**, *86*, 4314−4317.
(22) Nakayama, M.; Kotobuki, M.; Munakata, H.; Nogami, M.; Kanamura, K. First-principles density functional calculation of electrochemical stability of fast Li ion conducting garnet-type oxides. *Phys. Chem. Chem. Phys.* **2012**, *14*, 10008−10014.
(23) Ishikawa, R.; Mishra, R.; Lupini, A. R.; Findlay, S. D.; Taniguchi, T.; Pantelides, S. T.; Pennycook, S. J. Direct Observation of Dopant Atom Diffusion in a Bulk Semiconductor Crystal Enhanced by a Large Size Mismatch. *Phys. Rev. Lett.* **2014**, *113*, 155501.
(24) Lehtinen, O.; Kurasch, S.; Krasheninnikov, A. V.; Kaiser, U. Atomic scale study of the life cycle of a dislocation in graphene from birth to annihilation. *Nat. Commun.* **2013**, *4*, 2098.
(25) Warner, J. H.; Margine, E. R.; Mukai, M.; Robertson, A. W.; Giustino, F.; Kirkland, A. I. Dislocation-Driven Deformations in Graphene. *Science* **2012**, *337*, 209−212.
(26) Lin, Y.-C.; Dumcenco, D. O.; Huang, Y.-S.; Suenaga, K. Atomic mechanism of the semiconducting-to-metallic phase transition in single-layered MoS_2. *Nat. Nanotechnol.* **2014**, *9*, 391−396.
(27) Su, D.; Wang, F.; Ma, C.; Jiang, N. Engineering Nano-composite $Li_4Ti_5O_{12}$ anodes via scanning electron-probe fabrication. *Nano Energy* **2013**, *2*, 343−350.
(28) Pennycook, T. J.; Jones, L.; Pettersson, H.; Coelho, J.; Canavan, M.; Mendoza-Sanchez, B.; Nicolosi, V.; Nellist, P. D. Atomic scale dynamics of a solid state chemical reaction directly determined by annular dark-field electron microscopy. *Sci. Rep.* **2014**, *4*, 7555.
(29) Lu, P.; Yan, P.; Romero, E.; Spoerke, E. D.; Zhang, J.-G.; Wang, C.-M. Observation of Electron-Beam-Induced Phase Evolution Mimicking the Effect of the Charge-Discharge Cycle in Li-Rich Layered Cathode Materials Used for Li Ion Batteries. *Chem. Mater.* **2015**, *27*, 1375−1380.
(30) Gao, X.; Ikuhara, Y. H.; Fisher, C. A. J.; Moriwake, H.; Kuwabara, A.; Oki, H.; Kohama, K.; Yoshida, R.; Huang, R.; Ikuhara, Y. Structural Distortion and Compositional Gradients Adjacent to Epitaxial $LiMn_2O_4$ Thin Film Interfaces. *Adv. Mater. Interfaces* **2014**, *1*, 10.
(31) Urban, A.; Lee, J.; Ceder, G. The Configurational Space of Rocksalt-Type Oxides for High-Capacity Lithium Battery Electrodes. *Adv. Energy Mater.* **2014**, *4*, 1400478.
(32) Wei, Z.; Xia, Y.; Qiu, B.; Zhang, Q.; Han, S.; Liu, Z. Correlation between transition metal ion migration and the voltage ranges of electrochemical process for lithium-rich manganese-based material. *J. Power Sources* **2015**, *281*, 7−10.
(33) Wang, Z. L.; Kang, Z. C. *Functional and Smart Materials: Structural Evolution and Structure Analysis*; Plenum Press: New York, 1998.
(34) Tachibana, M.; Tojo, T.; Kawaji, H.; Atake, T.; Yonemura, M.; Kanno, R. Heat capacity of $LiMn_2O_{4-\delta}$: Effect of oxygen content on charge and magnetic ordering. *Phys. Rev. B: Condens. Matter Mater. Phys.* **2003**, *68*, 094421.

DOI: 10.1021/acs.chemmater.6b03659
Chem. Mater. 2017, 29, 1006−1013